

Hierarchical theories for a linearised stability analysis of thin-walled beams with open and closed cross-section

Gaetano Giunta^{*1}, Salim Belouettar^{1a}, Fabio Biscani^{1b} and Erasmo Carrera^{2c}

¹Centre de Recherche Public Henri Tudor, 29, av. John F. Kennedy,
L-1855, Luxembourg-Kirchberg, Luxembourg.

²Politecnico di Torino, 24, c.so Duca degli Abruzzi, 10129, Turin, Italy

(Received December 9, 2013, December 14, 2013, Accepted January 14, 2014)

Abstract. A linearised buckling analysis of thin-walled beams is addressed in this paper. Beam theories formulated according to a unified approach are presented. The displacement unknown variables on the cross-section of the beam are approximated via Mac Laurin's polynomials. The governing differential equations and the boundary conditions are derived in terms of a fundamental nucleo that does not depend upon the expansion order. Classical beam theories such as Euler-Bernoulli's and Timoshenko's can be retrieved as particular cases. Slender and deep beams are investigated. Flexural, torsional and mixed buckling modes are considered. Results are assessed toward three-dimensional finite element solutions. The numerical investigations show that classical and lower-order theories are accurate for flexural buckling modes of slender beams only. When deep beams or torsional buckling modes are considered, higher-order theories are required.

Keywords: beam structure; hierarchical modelling; closed form solution; buckling load

1. Introduction

Thin-walled beams are widely used as primary and secondary elements in structures of civil, mechanical and space engineering. The accurate prediction of the buckling loads (and, in particular, of the critical one) is mandatory for a safe and effective design. Stability analysis of beams represents, therefore, an interesting and important research topic.

To the best of the authors' knowledge, Wagner (1929, 1936), Goodier (1942), Timoshenko (1945), Timoshenko and Goodier (1970), Bleich (1952) and Vlasov (1959) are the pioneers of the theory of thin-walled beams stability. The governing differential equations were derived from either geometric/equilibrium considerations or the principle of stationary potential energy. Within the framework of Euler-Bernoulli's kinematic model, Nishino *et al.* (1977) proposed a variational formulation based upon the Principle of Virtual Displacements (PVD). Saucha and Rados (2001) presented a review on Vlasov's theory of stability also discussing some relations among the

*Corresponding author, Ph.D., E-mail: gaetano.giunta@tudor.lu

^a Ph.D., E-mail: salim.belouettar@tudor.lu

^b Ph.D., E-mail: fabio.biscani@tudor.lu

^c Professor, E-mail: erasmo.carrera@polito.it

afore-mentioned models. Over the years, several improvements in classical models have been proposed to account for non-classical effects. Chen and Santathadaporn (1968) presented a survey of analytical models and experimental results for beams under a bi-axial loading. A general review on beam modelling was proposed by Kapania and Raciti (1989a,b) accounting for static, buckling, free-vibration and wave propagation analyses. A review on the boundary conditions effect on the stability of thin-walled elements was presented by Trahair (1993). Since the early works by Schardt (1983, 1989, 1994), a remarkable effort has been devoted to the development of a generalised beam theory formally compatible with Vlasov's model for the analysis, amongst the others, of unbranched and branched thin-walled beams in Dinis *et al.* (2006) and Gonçalves *et al.* (2009) and frames in Basaglia *et al.* (2009) and Camotim *et al.* (2010). Zhang and Tong (2004) modelled the beams via shell elements based on Kirchhoff (1850) and Love (1888) kinematic hypotheses. They obtained the total potential from the PVD and accounted also for the non-linear strain energy due to normal and shear transverse stresses. They investigated cantilever beams in Zhang and Tong (2008) by this approach. Mohri *et al.* (2001) formulated a model for the post-buckling analysis of thin-walled beams with mono- and bi-symmetric cross-sections. Non-linearities were assumed in the relations between bending moments and principal curvatures via a Maclaurin series expansion. An algebraic system was derived via Galerkin's method in which shortening, warping and coupling between torsion and bending were accounted for. Vlasov's theory was also obtained. As far as experimental investigation is concerned, the works by Beale *et al.* (2001), Put *et al.* (1999) and Paczos and Wasilewicz (2009) are worth to be mentioned.

A linearised analysis of thin-walled beams via hierarchical models is addressed in this paper. Models are derived via a Unified Formulation (UF) that has been previously derived for plates and shells in Carrera (2003), Carrera and Giunta (2009a,b) and extended to beams in Carrera and Giunta (2010), Carrera *et al.* (2010) and Giunta *et al.* (2011). Through a concise notation for the displacement field, the governing differential equations and the corresponding boundary conditions are reduced to a 'fundamental nucleo' that does not depend upon the approximation order. This latter can be assumed as a formulation free parameter. Displacement-based theories that account for non-classical effects, such as transverse shear and cross-section in- and out-of-plane warping, can be formulated. Coupled flexural-torsion buckling modes are predicted although no warping functions are explicitly assumed. Governing differential equations are solved via a Navier's closed form solution. Slender and deep beams (within the limit of elastic behaviour) are investigated. Since a linearised approach is used, the change in geometry due to pre-buckling deformation is disregarded. Open and closed thin-walled cross-sections with at least a symmetry axis are, therefore, considered. It is worth mentioning that this limitation is due to the approach to the buckling analysis and not to the theory formulation itself. The present models are validated towards three-dimensional FEM solutions.

2. Preliminaries

A beam is a structure whose axial extension (l) is predominant if compared to any other dimension orthogonal to it. The cross-section (Ω) is identified by intersecting the beam with planes that are orthogonal to its axis. A Cartesian reference system is adopted: y - and z -axis are two orthogonal directions laying on Ω . The x coordinate is coincident to the axis of the beam. It is bounded such that $0 \leq x \leq l$. Cross-sections obtained as the union of N_{Ω^k} non-overlapping rectangular sub-domains

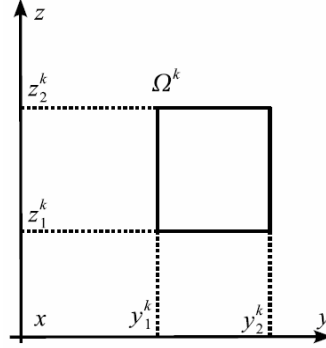


Fig. 1 Generic cross-section rectangular sub-domain

$$\Omega = \bigcup_{k=1}^{N_{\Omega^k}} \Omega^k \quad (1)$$

with

$$\Omega^k = \{(y, z): y_1^k \leq y \leq y_2^k; z_1^k \leq z \leq z_2^k\} \quad (2)$$

are considered, see Fig. 1. Terms $\{(y_i^k, z_j^k): i, j = 1, 2\}$ are the coordinates of the corner points of a k sub-domain. Through the paper, the superscript ' k ' represents a cross-section sub-domain index, while, as subscript, it stands for summation over the range $[1, N_{\Omega^k}]$. The cross-section is considered to be constant along the axial direction. The displacement field is

$$\mathbf{u}^T(x, y, z) = \{u_x(x, y, z) \quad u_y(x, y, z) \quad u_z(x, y, z)\} \quad (3)$$

where u_x , u_y and u_z are the displacement components along the the x -, y - and z -axis, respectively. Superscript ' T ' represents the transposition operator. Stress σ and strain ϵ vectors are grouped into vectors σ_n , ϵ_n that lay on the cross-section

$$\sigma_n^T = \{\sigma_{xx} \quad \sigma_{xy} \quad \sigma_{xz}\}, \quad \epsilon_n^T = \{\epsilon_{xx} \quad \epsilon_{xy} \quad \epsilon_{xz}\} \quad (4)$$

and σ_p , ϵ_p laying on planes orthogonal to Ω

$$\sigma_p^T = \{\sigma_{yy} \quad \sigma_{zz} \quad \sigma_{yz}\}, \quad \epsilon_p^T = \{\epsilon_{yy} \quad \epsilon_{zz} \quad \epsilon_{yz}\} \quad (5)$$

The linear strain-displacement geometrical relations are

$$\begin{aligned} \epsilon_n^{IT} &= \{u_{x,x} \quad u_{x,y} + u_{y,x} \quad u_{x,z} + u_{z,x}\} \\ \epsilon_p^{IT} &= \{u_{y,y} \quad u_{z,z} \quad u_{y,z} + u_{z,y}\} \end{aligned} \quad (6)$$

Subscripts ' x ', ' y ' and ' z ', when preceded by comma, represent derivation versus the corresponding spatial coordinate. A compact vectorial notation can be adopted for Eq. (6)

$$\begin{aligned}\boldsymbol{\varepsilon}_n^l &= \mathbf{D}_{np} \mathbf{u} + \mathbf{D}_{nx} \mathbf{u} \\ \boldsymbol{\varepsilon}_p^l &= \mathbf{D}_p \mathbf{u}\end{aligned}\quad (7)$$

\mathbf{D}_{np} , \mathbf{D}_{nx} , and \mathbf{D}_p are the following differential matrix operators

$$\mathbf{D}_p = \begin{bmatrix} 0 & 0 & 0 \\ \frac{\partial}{\partial y} & 0 & 0 \\ \frac{\partial}{\partial z} & 0 & 0 \end{bmatrix} \quad \mathbf{D}_{nx} = \mathbf{I} \frac{\partial}{\partial x} \quad \mathbf{D}_p = \begin{bmatrix} 0 & \frac{\partial}{\partial y} & 0 \\ 0 & 0 & \frac{\partial}{\partial z} \\ 0 & \frac{\partial}{\partial z} & \frac{\partial}{\partial y} \end{bmatrix} \quad (8)$$

where \mathbf{I} is the unit matrix. Geometric non-linearities are introduced in the axial strain in a Green-Lagrange sense (see [27])

$$\varepsilon_{xx}^{nl} = \frac{1}{2} (u_{x,x}^2 + u_{y,x}^2 + u_{z,x}^2) \quad (9)$$

Under the hypothesis of linear elastic materials, the generalised Hooke law holds. According to Eqs. (4) and (5), it reads

$$\begin{aligned}\boldsymbol{\sigma}_p &= \mathbf{C}_{pp} \boldsymbol{\varepsilon}_p^l + \mathbf{C}_{pn} \boldsymbol{\varepsilon}_n^l \\ \boldsymbol{\sigma}_n &= \mathbf{C}_{np} \boldsymbol{\varepsilon}_p^l + \mathbf{C}_{nn} \boldsymbol{\varepsilon}_n^l\end{aligned}\quad (10)$$

Matrixes \mathbf{C}_{pp} , \mathbf{C}_{pn} , \mathbf{C}_{np} and \mathbf{C}_{nn} in Eq. (10) are

$$\mathbf{C}_{pp} = \begin{bmatrix} C_{22} & C_{23} & 0 \\ C_{23} & C_{33} & 0 \\ 0 & 0 & C_{44} \end{bmatrix} \quad \mathbf{C}_{pn} = \mathbf{C}_{np}^T = \begin{bmatrix} C_{12} & 0 & 0 \\ C_{13} & 0 & 0 \\ 0 & 0 & 0 \end{bmatrix} \quad \mathbf{C}_{nn} = \begin{bmatrix} C_{11} & 0 & 0 \\ 0 & C_{66} & 0 \\ 0 & 0 & C_{55} \end{bmatrix} \quad (11)$$

where the coefficients C_{ij} are

$$\begin{aligned}C_{11} = C_{22} = C_{33} &= \frac{1-\nu}{(1+\nu)(1-2\nu)} E & C_{12} = C_{13} = C_{23} &= \frac{\nu}{(1+\nu)(1-2\nu)} E \\ C_{44} = C_{55} = C_{66} &= \frac{E}{2(1+\nu)}\end{aligned}\quad (12)$$

being E the Young modulus and ν the Poisson ratio.

3. Hierarchical beam theories

The variation of the displacement field over the cross-section is a-priori postulated. Several displacement-based theories can be formulated on the basis of the following generic kinematic

Table 1 Mac Laurin’s polynomials terms via Pascal’s triangle

N	N_u	F_τ
0	1	$F_1 = 1$
1	3	$F_2 = y \quad F_3 = z$
2	6	$F_4 = y^2 \quad F_5 = yz \quad F_6 = z^2$
3	10	$F_7 = y^3 \quad F_8 = y^2z \quad F_9 = yz^2 \quad F_{10} = z^3$
...
N	$\frac{(N+1)(N+2)}{2}$	$F_{\frac{N^2+N+2}{2}} = y^N \quad F_{\frac{N^2+N+4}{2}} = y^{N-1}z \quad \dots \quad F_{\frac{N(N+3)}{2}} = yz^{N-1} \quad F_{\frac{(N+1)(N+2)}{2}} = z^N$

field

$$\mathbf{u}(x, y, z) = F_\tau(y, z)\mathbf{u}_\tau(x) \text{ with } \tau = 1, 2, \dots, N_u \tag{13}$$

where N_u stands for the number of approximating terms. It depends on the approximation order N that is a free parameter of the present formulation. The compact expression in Eq. (13) is based on Einstein’s notation: twice repeated subscripts indicate summation. Thanks to this notation, problem’s governing differential equations and boundary conditions can be derived in terms of a single ‘fundamental nucleo’. The complexity related to higher than classical approximation terms is tackled and the theoretical formulation is valid for the generic approximation order and approximating functions $F_\tau(y, z)$. In this paper, the functions F_τ are assumed to be Maclaurin’s polynomials. This choice is inspired by the classical beam models. N_u and F_τ as functions of N can be obtained via Pascal’s triangle as shown in Table 1. The actual governing differential equations and boundary conditions due to a fixed approximation order and polynomials type are obtained straightforwardly via summation of the nucleo corresponding to each term of the expansion. According to the previous choice for the approximating functions, a generic, N -order displacement field is

$$\begin{aligned} u_x &= u_{x1} + u_{x2}y + u_{x3}z + \dots + u_{x\bar{N}}y^{\bar{N}} + \dots + u_{xN_{tot}}z^N \\ u_y &= u_{y1} + u_{y2}y + u_{y3}z + \dots + u_{y\bar{N}}y^{\bar{N}} + \dots + u_{yN_{tot}}z^N \\ u_z &= u_{z1} + u_{z2}y + u_{z3}z + \dots + u_{z\bar{N}}y^{\bar{N}} + \dots + u_{zN_{tot}}z^N \end{aligned} \tag{14}$$

with $\bar{N} = \frac{N^2 + N + 2}{2}$ and $N_{tot} = \frac{(N+1)(N+2)}{2}$

As far as the first-order approximation order is concerned, the kinematic field is

$$\begin{aligned} u_x &= u_{x1} + u_{x2}y + u_{x3}z \\ u_y &= u_{y1} + u_{y2}y + u_{y3}z \\ u_z &= u_{z1} + u_{z2}y + u_{z3}z \end{aligned} \tag{15}$$

Classical models, such as Timoshenko’s beam theory (TBT)

$$\begin{aligned}
u_x &= u_{x1} + u_{x2}y + u_{x3}z \\
u_y &= u_{y1} \\
u_z &= u_{z1}
\end{aligned} \tag{16}$$

and Euler-Bernoulli beam theory (EBT)

$$\begin{aligned}
u_x &= u_{x1} - u_{y1,x}y - u_{z1,x}z \\
u_y &= u_{y1} \\
u_z &= u_{z1}
\end{aligned} \tag{17}$$

are straightforwardly derived from the first-order approximation model. In TBT, no shear correction coefficient is considered, since it depends upon several parameters, such as the geometry of the cross-section (see, for instance, Cowper (1966) and Murty (1970)). Higher order models yield a more detailed description of the shear mechanics (no shear correction coefficient is required), of the in- and out-of-section deformations, of the coupling of the spatial directions due to Poisson's effect and of the torsional mechanics than classical models do. EBT theory neglects them all, since it was formulated to describe the bending mechanics. TBT model accounts for constant shear stress and strain components. In the case of classical models and first-order approximation, the material stiffness coefficients should be corrected in order to contrast a phenomenon known in literature as Poisson's locking (see Carrera and Brischetto (2008a,b)).

4. Governing equations

The strong form of the governing differential equations and the boundary conditions are obtained via Euler's method of adjacent states of equilibrium upon the assumption that the pre-buckling deformation can be neglected. The Principle of Virtual Displacements reads

$$\delta L_i - \delta L_{\sigma_{xx}^0} = 0 \tag{18}$$

where δ stands for a virtual variation, L_i represents the strain energy and $L_{\sigma_{xx}^0}$ is the work done by an axial pre-stress σ_{xx}^0 on the corresponding non-linear strain ε_{xx}^{nl} . The axial pre-stress is assumed constant along the beam axis and it does not change in magnitude nor in direction during buckling.

4.1 Virtual variation of the strain energy

According to the grouping of the stress and strain components in Eqs. (4) and (5), the virtual variation of the strain energy is considered as sum of two contributes

$$\delta L_i = \int_l \left(\int_{\Omega^k} \delta \varepsilon_n^T \sigma_n d\Omega \right)_k dx + \int_l \left(\int_{\Omega^k} \delta \varepsilon_p^T \sigma_p d\Omega \right)_k dx \tag{19}$$

By substitution of the geometrical relations, Eq. (7), the material constitutive equations,

Eq. (10), and the unified hierarchical approximation of the displacements, Eq. (13), and after integration by parts, Eq. (19) reads

$$\begin{aligned}
 \delta L_i = & \int_l \delta \mathbf{u}_\tau^T \left\{ \int_{\Omega^k} \left[(\mathbf{D}_{np} F_\tau)^T \left[\mathbf{C}_{np}^k (\mathbf{D}_p F_s \mathbf{I}) + \mathbf{C}_{nn}^k (\mathbf{D}_{np} F_s \mathbf{I} + F_s \mathbf{D}_{nx}) \right] \right. \right. \\
 & \left. \left. + (\mathbf{D}_p F_\tau)^T \left[\mathbf{C}_{pp}^k (\mathbf{D}_p F_s \mathbf{I}) + \mathbf{C}_{pn}^k (\mathbf{D}_{np} F_s \mathbf{I} + F_s \mathbf{D}_{nx}) \right] \right] \right. \\
 & \left. - \mathbf{D}_{nx}^T \left[\mathbf{C}_{np}^k (\mathbf{D}_p F_s \mathbf{I}) + \mathbf{C}_{nn}^k (\mathbf{D}_{np} F_s \mathbf{I} + F_s \mathbf{D}_{nx}) \right] \right\} d\Omega \Big|_k \mathbf{u}_s dx \\
 & + \delta \mathbf{u}_\tau^T \left\{ \int_{\Omega^k} \left[\mathbf{C}_{np}^k (\mathbf{D}_p F_s \mathbf{I}) + \mathbf{C}_{nn}^k (\mathbf{D}_{np} F_s \mathbf{I} + F_s \mathbf{D}_{nx}) \right] d\Omega \right\}_k \mathbf{u}_s \Big|_{x=0}^{x=l}
 \end{aligned} \quad (20)$$

and in a compact vectorial form

$$\delta L_i = \int_l \delta \mathbf{u}_\tau^T \bar{\mathbf{K}}^{\tau s} \mathbf{u}_s dx + \delta \mathbf{u}_\tau^T \bar{\mathbf{\Pi}}^{\tau s} \mathbf{u}_s \Big|_{x=0}^{x=l} \quad (21)$$

The components of the differential linear stiffness matrix $\bar{\mathbf{K}}^{\tau s}$ are

$$\begin{aligned}
 \bar{K}_{xx}^{\tau s} &= J_{\tau,ys,y}^{66} + J_{\tau,zs,z}^{55} - J_{\tau s}^{11} \frac{\partial^2}{\partial x^2} & \bar{K}_{xy}^{\tau s} &= (J_{\tau,ys}^{66} - J_{\tau s,y}^{12}) \frac{\partial}{\partial x} & \bar{K}_{xz}^{\tau s} &= (J_{\tau,zs}^{55} - J_{\tau s,z}^{13}) \frac{\partial}{\partial x} \\
 \bar{K}_{yy}^{\tau s} &= J_{\tau,ys,y}^{22} + J_{\tau,zs,z}^{44} - J_{\tau s}^{66} \frac{\partial^2}{\partial x^2} & \bar{K}_{yx}^{\tau s} &= (J_{\tau,ys}^{12} - J_{\tau s,y}^{66}) \frac{\partial}{\partial x} & \bar{K}_{yz}^{\tau s} &= J_{\tau,ys,z}^{23} + J_{\tau,zs,y}^{44} \\
 \bar{K}_{zz}^{\tau s} &= J_{\tau,ys,y}^{44} + J_{\tau,zs,z}^{33} - J_{\tau s}^{55} \frac{\partial^2}{\partial x^2} & \bar{K}_{zx}^{\tau s} &= (J_{\tau,zs}^{13} - J_{\tau s,z}^{55}) \frac{\partial}{\partial x} & \bar{K}_{zy}^{\tau s} &= J_{\tau,ys,z}^{44} + J_{\tau,zs,y}^{23}
 \end{aligned} \quad (22)$$

The generic term $J_{\tau(\phi)s(\xi)}^{gh}$ is a cross-section moment

$$J_{\tau(\phi)s(\xi)}^{gh} = \left(\int_{\Omega^k} C_{gh}^k F_{\tau(\phi)} F_{s(\xi)} d\Omega \right)_k \quad (23)$$

Since the material is isotropic and the approximating functions are the elements of the classical polynomial base, the previous equation can be rewritten as

$$J_{\tau(\phi)s(\xi)}^{gh} = \left(C_{gh}^k k_y k_z \int_{\Omega^k} y^{n_y} z^{n_z} d\Omega \right)_k \quad (24)$$

where k_y , k_z , n_y and n_z are constant depending upon indexes τ and s as in Table 1 and whether differentiation with respect to y and z should be performed or not. The analytical

solution of integral in Eq. (23) is

$$J_{\tau(\varphi)s(\bar{z})}^{gh} = \left\{ C_{gh}^k \frac{k_y}{n_y + 1} \left[(y_2^k)^{n_y+1} + (y_1^k)^{n_y+1} \right] \frac{k_z}{n_z + 1} \left[(z_2^k)^{n_z+1} + (z_1^k)^{n_z+1} \right] \right\}_k \quad (25)$$

As far as the boundary conditions are concerned, the components of $\bar{\Pi}^{\tau s}$ are

$$\begin{aligned} \bar{\Pi}_{xx}^{\tau s} &= J_{\tau s}^{11} \frac{\partial}{\partial x} & \bar{\Pi}_{xy}^{\tau s} &= J_{\tau s, y}^{12} & \bar{\Pi}_{xz}^{\tau s} &= J_{\tau s, z}^{13} \\ \bar{\Pi}_{yy}^{\tau s} &= J_{\tau s}^{66} \frac{\partial}{\partial x} & \bar{\Pi}_{yx}^{\tau s} &= J_{\tau s, y}^{66} & \bar{\Pi}_{yz}^{\tau s} &= 0 \\ \bar{\Pi}_{zz}^{\tau s} &= J_{\tau s}^{55} \frac{\partial}{\partial x} & \bar{\Pi}_{zx}^{\tau s} &= J_{\tau s, z}^{55} & \bar{\Pi}_{zy}^{\tau s} &= 0 \end{aligned} \quad (26)$$

4.2 Virtual work of the axial pre-stress

The virtual work of the axial pre-stress is

$$\delta L_{\sigma_{xx}^0} = \int_l \left(\int_{\Omega^k} \delta \varepsilon_{xx}^{nl} \sigma_{xx}^0 d\Omega \right) dx \quad (27)$$

Upon substitution of Eqs. (9) and (13) and after integration by parts, Eq. (2) becomes

$$\delta L_{\sigma_{xx}^0} = -\sigma_{xx}^0 \int_l \delta \mathbf{u}_{\tau}^T \left(\int_{\Omega^k} F_{\tau} F_s d\Omega \right)_k \mathbf{I} \frac{\partial^2}{\partial x^2} \mathbf{u}_s dx + \sigma_{xx}^0 \delta \mathbf{u}_{\tau}^T \left(\int_{\Omega^k} F_{\tau} F_s d\Omega \right)_k \mathbf{I} \frac{\partial}{\partial x} \mathbf{u}_s \Big|_{x=0}^{x=l} \quad (28)$$

In a compact vectorial form

$$\delta L_{\sigma_{xx}^0} = -\sigma_{xx}^0 \int_l \delta \mathbf{u}_{\tau}^T \bar{\mathbf{K}}_{\sigma_{xx}^0}^{\tau s} \mathbf{u}_s dx + \sigma_{xx}^0 \delta \mathbf{u}_{\tau}^T \bar{\Pi}_{\sigma_{xx}^0}^{\tau s} \mathbf{u}_s \Big|_{x=0}^{x=l} \quad (29)$$

The components of the differential geometric stiffness matrix $\bar{\mathbf{K}}_{\sigma_{xx}^0}^{\tau s}$ are

$$\bar{\mathbf{K}}_{\sigma_{xx}^0}^{\tau s} = \delta_{ij} J_{\tau s} \frac{\partial^2}{\partial x^2} \text{ with } i, j = x, y, z \quad (30)$$

where δ_{ij} is Kronecker's delta and

$$J_{\tau s} = \left(\int_{\Omega^k} F_{\tau} F_s d\Omega \right)_k \quad (31)$$

The components of $\bar{\Pi}_{\sigma_{xx}^0}^{\tau s}$ are

$$\bar{\Pi}_{\sigma_{xx}^0 ij}^{\tau s} = \delta_{ij} J_{\tau s} \frac{\partial}{\partial x} \text{ with } i, j = x, y, z \quad (32)$$

4.3 Governing equations' fundamental nucleo

The explicit form of the fundamental nucleo of the governing equations is

$$\begin{aligned} \delta u_{x\tau} : & -\left(J_{\tau s}^{11} - \sigma_{xx}^0 J_{\tau s}\right) u_{xs,xx} + \left(J_{\tau,zs,z}^{55} + J_{\tau,ys,y}^{66}\right) u_{xs} + \left(J_{\tau,ys}^{66} - J_{\tau s,y}^{12}\right) u_{ys,x} + \left(J_{\tau,zs}^{55} - J_{\tau s,z}^{13}\right) u_{zs,x} = 0 \\ \delta u_{y\tau} : & \left(J_{\tau,ys}^{12} - J_{\tau s,y}^{66}\right) u_{xs,x} - \left(J_{\tau s}^{66} - \sigma_{xx}^0 J_{\tau s}\right) u_{ys,xx} + \left(J_{\tau,ys,y}^{22} + J_{\tau,zs,z}^{44}\right) u_{ys} + \left(J_{\tau,ys,z}^{23} + J_{\tau,zs,y}^{44}\right) u_{zs} = 0 \\ \delta u_{z\tau} : & \left(J_{\tau,zs}^{13} - J_{\tau s,z}^{55}\right) u_{xs,x} + \left(J_{\tau,zs,y}^{23} + J_{\tau,ys,z}^{44}\right) u_{ys} - \left(J_{\tau s}^{55} - \sigma_{xx}^0 J_{\tau s}\right) u_{zs,xx} + \left(J_{\tau,zs,z}^{33} + J_{\tau,ys,y}^{44}\right) u_{zs} = 0 \end{aligned} \quad (33)$$

The boundary conditions are

$$\begin{aligned} \delta u_{x\tau} \left[\left(J_{\tau s}^{11} - \sigma_{xx}^0 J_{\tau s}\right) u_{xs,x} + J_{\tau s,y}^{12} u_{ys} + J_{\tau s,z}^{13} u_{zs} \right] \Big|_{x=0}^{x=l} &= 0 \\ \delta u_{y\tau} \left[J_{\tau s,y}^{66} u_{xs} + \left(J_{\tau s}^{66} - \sigma_{xx}^0 J_{\tau s}\right) u_{ys,x} \right] \Big|_{x=0}^{x=l} &= 0 \\ \delta u_{z\tau} \left[J_{\tau s,z}^{55} u_{xs} + \left(J_{\tau s}^{55} - \sigma_{xx}^0 J_{\tau s}\right) u_{zs,x} \right] \Big|_{x=0}^{x=l} &= 0 \end{aligned} \quad (34)$$

For a fixed approximation order, the nucleo has to be expanded versus the indexes τ and s in order to obtain the governing equations and the boundary conditions of the desired model.

5. Closed form analytical solution

The differential equations are solved via a Navier type solution. Simply supported beams are, therefore, investigated. The following displacement field is adopted

$$\begin{aligned} u_x &= U_{x\tau} F_{\tau} \cos(\alpha x) \\ u_y &= U_{y\tau} F_{\tau} \sin(\alpha x) \\ u_z &= U_{z\tau} F_{\tau} \sin(\alpha x) \end{aligned} \quad (35)$$

where α is

$$\alpha = \frac{m\pi}{l} \text{ with } m \in N^* \quad (36)$$

m representing the half-wave number along the beam axis. $\{U_{i\tau} : i = x, y, z\}$ are the maximal

amplitudes of the displacement components. The displacement field in Eq. (35) satisfies the boundary conditions since

$$\begin{aligned} u_{x\tau x}(0) &= u_{x\tau x}(l) = 0 \\ u_{y\tau}(0) &= u_{y\tau}(l) = 0 \\ u_{z\tau}(0) &= u_{z\tau}(l) = 0 \end{aligned} \quad (37)$$

Upon substitution of Eq. (35) into Eq. (33), the fundamental nucleo of the algebraic eigensystem is obtained

$$\delta \mathbf{U}_\tau : \left(\mathbf{K}^{\tau s} - \sigma_{xx}^0 \mathbf{K}_{\sigma_{xx}^0}^{\tau s} \right) \mathbf{U}_s = 0 \quad (38)$$

and

$$\begin{aligned} K_{xx}^{\tau s} &= J_{\tau,ys,y}^{66} + J_{\tau,zs,z}^{55} + \alpha^2 J_{\tau s}^{11} & K_{xy}^{\tau s} &= \alpha \left(J_{\tau,ys}^{66} - J_{\tau s,y}^{12} \right) & K_{xz}^{\tau s} &= \alpha \left(J_{\tau,zs}^{55} - J_{\tau s,z}^{13} \right) \\ K_{yy}^{\tau s} &= J_{\tau,ys,y}^{22} + J_{\tau,zs,z}^{44} + \alpha^2 J_{\tau s}^{66} & K_{yx}^{\tau s} &= \alpha \left(J_{\tau s,y}^{66} - J_{\tau,ys}^{12} \right) & K_{yz}^{\tau s} &= J_{\tau,ys,z}^{23} + J_{\tau,zs,y}^{44} \\ K_{zz}^{\tau s} &= J_{\tau,ys,y}^{44} + J_{\tau,zs,z}^{33} + \alpha^2 J_{\tau s}^{55} & K_{zx}^{\tau s} &= \alpha \left(J_{\tau s,z}^{55} - J_{\tau,zs}^{13} \right) & K_{zy}^{\tau s} &= J_{\tau,ys,z}^{44} + J_{\tau,zs,y}^{23} \end{aligned} \quad (39)$$

and

$$K_{\sigma_{xx}^0}^{\tau s} = \delta_{ij} \alpha^2 J_{\tau s} \text{ with } i, j = x, y, z \quad (40)$$

For a fixed approximation order and m , the eigensystem has to be assembled according to the summation indexes τ and s . Its solution yields as many eigenvalues (or buckling loads) and eigenvectors (or buckling modes) as the degrees of freedom of the model.

6. Numerical results and discussion

Beams made of the aluminium alloy 7075-T6 are considered. Mechanical properties are: Young's modulus equal to 71700 MPa, Poisson's ratio equal to 0.3 and yield stress (σ_y) equal to 503 MPa. Analyses are carried out considering open and closed thin-walled cross-sections. The ratio between a representative dimension of the cross-section ($a = 0.1$ m) and the walls thickness (h) is 20. The minimum value of the length-to-side ratio ($l/a = 15$) is such that a linear stress-strain relation holds. Slender beams ($l/a = 100$) are also accounted for. As far as validation is concerned, results are compared with FEM three-dimensional solutions obtained via the commercial code Ansys. The quadratic three-dimensional "SOLID186" element is used. For each considered case, a convergence analysis of the FEM reference solution versus the element sides length (Δx_e , Δy_e and Δz_e) is presented. Although the three-dimensional FEM solution and the analytical one are different in nature some considerations about computational time and effort can be addressed. The degrees of freedom of the three-dimensional FEM models are about $7 \cdot 10^4$ for the coarsest considered mesh, whereas, in the case of a tenth-order analytical model, they are 198.

Table 2 Box beam critical buckling load [MPa] via three-dimensional FEM analyses

l/a	$\Delta x_e, \Delta y_e, \Delta z_e$ [mm]	σ_{xx}^0 [MPa]	DOFs 10^4
100	100, 5.0, 5.0	10.640	15.8
	50, 5.0, 5.0	10.651	31.8
50	50, 5.0, 5.0	42.460	15.8
	25, 5.0, 5.0	42.497	31.8
20	25, 5.0, 5.0	261.05	12.6
	25, 2.5, 2.5	261.04	39.8
15	25, 5.0, 5.0	457.04	9.5
	25, 2.5, 2.5	457.01	29.8

Table 3 Box beam critical buckling load [MPa]

l/a	100	50	20	15
FEM 3D	10.651	42.497	261.04	457.01
$N = 4$	10.664, 0.12 ^a	42.551, 0.13	261.34, 0.11	457.31, 0.07
$N = 3$	10.664, 0.12	42.551, 0.13	261.34, 0.11	457.32, 0.07
$N = 2$	10.668, 0.16	42.605, 0.25	261.36, 0.89	463.51, 1.42
TBT	10.668, 0.16	42.604, 0.25	261.32, 0.87	463.40, 1.40
EBT	10.672, 0.20	42.669, 0.40	265.85, 1.84	471.26, 3.12

a: Absolute value of the percentage relative error

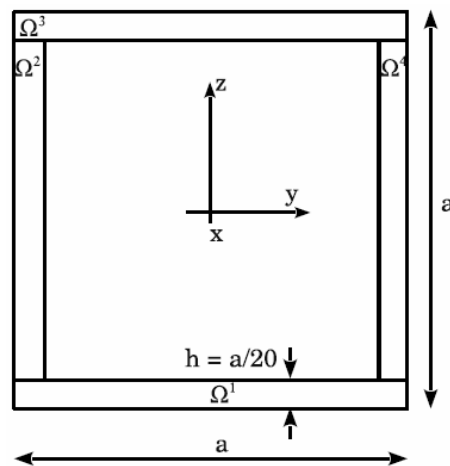


Fig. 2 Box-beam cross-section geometry

6.1 Box cross-section

Beams with the box cross-section shown in Fig. 2 are firstly investigated. Table 2 presents the results obtained by FEM three-dimensional simulations for the first buckling load that corresponds

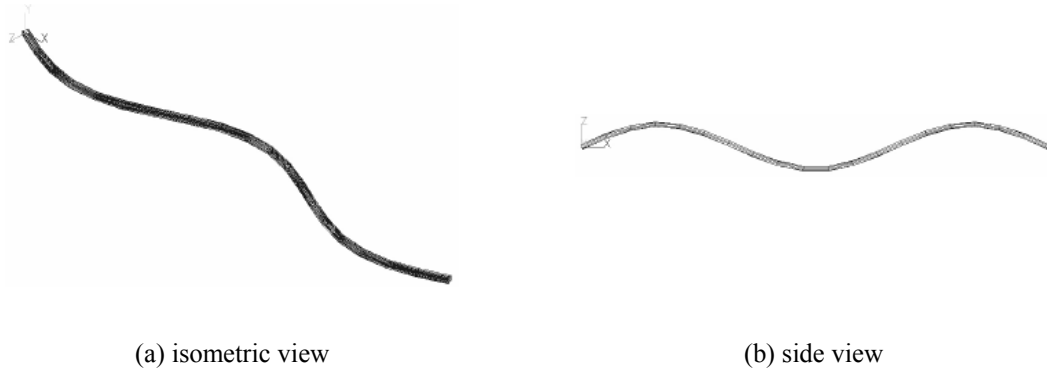


Fig. 3 Bending mode with three half-waves via a $N = 6$ model, box-beam, $l/a = 100$

Table 4 Box beam critical buckling load [MPa] versus the half-wave number, $l/a = 100$

m	1	2	3	4
FEM 3D	10.651	42.443	95.008	167.78
$N = 6$	10.664, 0.12 ^a	42.540, 0.23	95.287, 0.29	168.34, 0.33
$N = 5$	10.664, 0.12 ^a	42.540, 0.23	95.287, 0.29	168.34, 0.33
$N = 4$	10.664, 0.12 ^a	42.551, 0.25	95.339, 0.35	168.50, 0.43
$N = 3$	10.664, 0.12	42.551, 0.25	95.339, 0.35	168.50, 0.43
$N = 2$	10.668, 0.16	42.604, 0.38	95.607, 0.63	169.34, 0.93
TBT	10.668, 0.16	42.603, 0.38	95.602, 0.63	169.33, 0.92
EBT	10.672, 0.20	42.669, 0.40	95.934, 0.97	170.37, 1.54

a: Absolute value of the percentage relative error.

Table 5 First three buckling loads via three-dimensional FEM analysis, I-shaped cross-section beams

l/a	$\Delta x_e, \Delta y_e, \Delta z_e$ [mm]	σ_{xx}^0 [MPa]			DOFs 10^4
		Mode I ^a	Mode II ^b	Mode III ^c	
100	100, 5.0, 5.0	4.0607	- ^d	12.456	12.6
	50, 5.0, 5.0	4.0645	-	12.469	25.4
50	50, 5.0, 5.0	16.224	115.44	49.603	12.6
	25, 5.0, 5.0	16.236	115.54	49.649	25.4
20	25, 5.0, 5.0	100.72	197.11	300.68	10.1
	25, 2.5, 2.5	100.72	196.58	300.65	30.6
15	25, 5.0, 5.0	177.99	272.04	-	7.5
	25, 2.5, 2.5	177.99	271.53	-	22.9

a: Bending on plane xz . b: Torsional mode.

c: Bending on plane xy . d: Buckling load higher than yielding load.

to a flexural mode. The results computed via the proposed Unified Formulation are shown in Table 3. As expected, in the case of slender beams ($l/a = 100$ and 10), classical theories yield accurate results. In the case of deep beam ($l/a = 15$), TBT overestimates the reference solution by

about 1.4%, whereas EBT does by about 3.1%. Higher-order theories yield accurate results. Table 4 presents the buckling load for several values of the half-wave number along the beam axis. A slender beam is considered. As the value of m increases, the accuracy of the classical theories becomes less and less accurate. Increasing N , the buckling loads converge to a value smaller than the three-dimensional FEM one by about 0.4% for all the considered values of m . The buckling mode with $m = 3$ and $N = 6$ is shown in Fig. 3.

6.2 I-Shaped cross-section

Beams with I-shaped cross-section are investigated. The cross-section geometry is shown in Fig. 4. Results obtained with the FEM three-dimensional solutions are presented in Table 5. Three different buckling modes are considered: flexural on plane xz , torsional and bending on plane xy . In the case of slender beam ($l/a = 100$), the buckling loads of the torsional mode is higher than the yielding load. The same applies for the flexural mode on plane xy in the case of deep beam ($l/a = 15$). Tables 6, 7 and 8 present the results computed via the proposed models for the considered buckling modes. In the case of the bending modes, the same comments made for beams with a box cross-section apply. Classical theories yield accurate results for slender beams, whereas

Table 6 Mode I (bending on plane xz) critical buckling load [MPa], I-shaped cross-section beams

l/a	100	50	20	15
FEM 3D	4.0645	16.236	100.72	177.99
$N = 14$	4.0702, 0.14 ^a	16.267, 0.19	101.04, 0.32	178.55, 0.31
$N = 10$	4.0704, 0.15	16.268, 0.20	101.06, 0.34	178.63, 0.36
$N = 6$	4.0704, 0.15	16.269, 0.20	101.12, 0.40	178.85, 0.48
$N = 5$	4.0705, 0.15	16.269, 0.20	101.13, 0.41	178.89, 0.51
$N = 4$	4.0707, 0.15	16.271, 0.22	101.22, 0.50	179.18, 0.67
$N = 3$	4.0706, 0.15	16.271, 0.22	101.22, 0.50	179.18, 0.67
$N = 2$	4.0707, 0.15	16.273, 0.23	101.29, 0.57	179.39, 0.79
TBT	4.0707, 0.15	16.272, 0.22	101.27, 0.55	179.33, 0.75
EBT	4.0714, 0.17	16.282, 0.28	101.64, 0.91	180.50, 1.41

a: Absolute value of the percentage relative error.

Table 7 Mode II (torsion) buckling load [MPa] via the proposed models, I-shaped cross-section beams. The values for $N \leq 7$ are not reported since they are higher than the yielding stress

l/a	50	20	15
FEM 3D	115.54	196.58	271.53
$N = 14$	136.81, 18.4 ^a	216.84, 10.3	290.14, 6.8
$N = 13$	149.38, 29.2	228.99, 16.4	301.94, 11.2
$N = 12$	149.39, 29.3	229.01, 16.5	301.95, 11.2
$N = 11$	168.84, 46.1	247.72, 26.0	320.02, 17.8
$N = 10$	168.85, 46.1	247.75, 26.0	320.05, 17.8
$N = 9$	250.22, 116.5	326.62, 66.1	396.78, 46.1
$N = 8$	250.27, 116.6	326.82, 66.2	397.05, 46.2

a: Absolute value of the percentage relative error.

Table 8 Mode III (bending on plane xy) buckling load [MPa], I-shaped cross-section beams

l/a	100	50	20
FEM 3D	12.469	49.649	300.65
$N = 6$	12.484, 0.12 ^a	49.711, 0.12	301.09, 0.15
$N = 5$	12.484, 0.12	49.711, 0.12	301.10, 0.15
$N = 4$	12.486, 0.14	49.734, 0.17	301.95, 0.43
$N = 3$	12.486, 0.14	49.734, 0.17	301.96, 0.44
$N = 2$	12.496, 0.22	49.890, 0.49	307.80, 2.38
TBT	12.496, 0.22	49.890, 0.49	307.78, 2.37
EBT	12.501, 0.26	49.980, 0.67	311.23, 3.52

a: Absolute value of the percentage relative error.

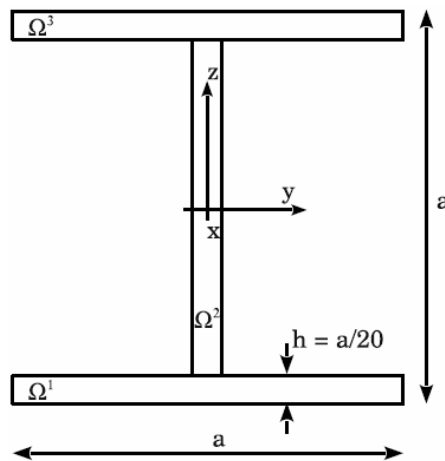


Fig. 4 I-shaped cross-section geometry

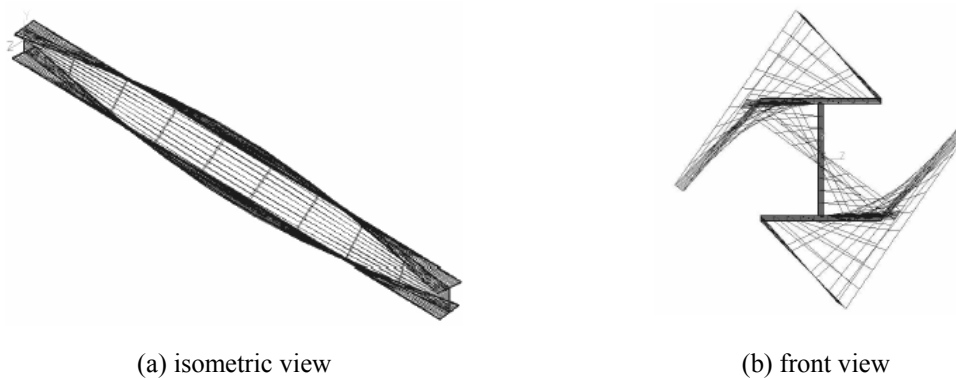


Fig. 5 Torsional mode via a $N = 12$ model, I-shaped cross-section beam, $l/a = 20$

they overestimate the buckling load by about 4% for deep beams. In the case of the torsional mode, classical and low-order theories are not accurate. By increasing N , the buckling load converges

towards the reference solution. In the case of $l/a = 50$, an expansion order as high as 14 yields a solution that is about the 18% higher than the FEM reference one. The difference is about 6.8% for deep beams ($l/a = 15$). Besides further increasing the expansion order, a possibility to improve the accuracy of the proposed models consists in a change in the approximation type for the kinematic field. A ‘layer-wise’ approximation (that is, locally over the cross-section sub-domains) can be used instead of a global one. It should be also noticed that for $N \leq 7$ the considered models all yield a torsional buckling load that is higher than the yielding stress. Fig. 5 shows the torsional mode as obtained by a 12-order approximation.

6.3 C-Shaped cross-section

Beams with C-shaped cross-section (as shown in Fig. 6) are finally investigated. Table 9 presents the convergence analysis for the FEM three-dimensional simulations. Two buckling

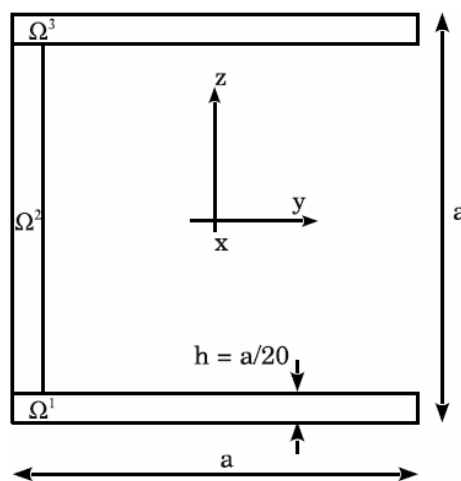


Fig. 6 C-shaped cross-section geometry

Table 9 First two buckling loadings via three-dimensional FEM analysis, C-shaped cross-section beams

l/a	$\Delta x_e, \Delta y_e, \Delta z_e$ [mm]	σ_{xx}^0 [MPa]		DOFs 10^4
		Mode I ^a	Mode II ^b	
100	100, 5.0, 5.0	9.4291	7.4677	12.2
	50, 5.0, 5.0	9.4393	7.4748	24.6
50	50, 5.0, 5.0	21.860	29.821	12.2
	25, 5.0, 5.0	21.882	29.845	24.6
20	25, 5.0, 5.0	55.454	- ^c	9.8
	25, 2.5, 2.5	55.374	-	30.6
15	25, 5.0, 5.0	81.425	-	7.3
	25, 2.5, 2.5	81.333	-	22.9

a: Coupled bending on plane xy and torsion. b: Bending on plane xz .

c: Buckling load higher than yielding load.

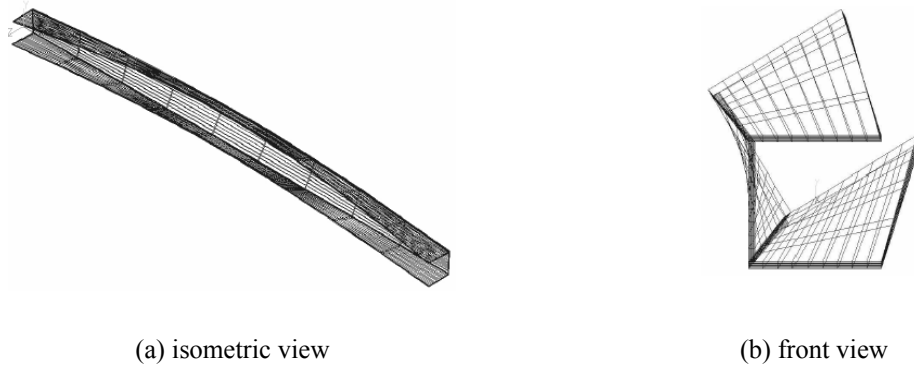


Fig. 7 Coupled bending-torsion mode via a $N = 12$ model, C-shaped cross-section beam, $l/a = 100$

Table 10 Mode I (coupled bending-torsion) buckling load [MPa], C-shaped cross-section beams

l/a	100	50	20	15
FEM 3D	9.4393	21.882	55.374	81.333
$N = 14$	9.6605, 2.34 ^a	22.929, 4.78	57.532, 3.90	83.784, 3.01
$N = 12$	9.7611, 3.41	23.447, 7.15	58.560, 5.75	84.907, 4.39
$N = 10$	10.175, 7.79	25.797, 17.8	63.592, 14.8	90.329, 11.0
$N = 8$	10.473, 10.9	27.737, 26.7	68.305, 23.3	95.495, 17.4
$N = 7$	11.081, 17.3	29.889, 36.5	82.946, 49.7	111.77, 37.4
$N = 6$	11.822, 25.2	29.889, 36.5	125.65, 126.9	163.57, 101.1
$N = 5$	12.174, 28.9	29.889, 36.5	180.55, 226.0	244.22, 200.2
$N = 4$	12.227, 29.5	29.890, 36.6	184.71, 233.5	267.99, 229.5
$N = 3$	12.479, 32.2	29.894, 36.6	184.87, 233.8	325.50, 300.2
$N = 2$	12.495, 32.3	29.907, 36.6	185.37, 234.7	327.06, 302.1
TBT	12.496, 32.3	29.910, 36.6	185.48, 234.9	327.38, 302.5
EBT	12.501, 32.4	29.942, 36.8	186.73, 237.2	331.29, 307.3

a: Absolute value of the percentage relative error .

b: Pure flexural mode on plane xy .

modes are considered: a pure flexural mode on plane xz and a combination of bending on plane xy and torsion (as shown in Fig. 7). The order of apparition of these two modes depends upon the ratio l/a . In the case of slender beam ($l/a = 100$), the first buckling mode is pure bending, whereas for all the other considered values of l/a the bending-torsion mixed mode is the critical one.

Furthermore, in the case of $l/a = 15$ and 20, the buckling load of the pure flexural mode is higher than the yielding stress. Table 10 presents the results computed via the proposed UF for the mixed buckling mode. Classical and low-order theories provide very poor results. For EBT and TBT, the torsion component of the mode is neglected and a pure bending is predicted. The error is about 32% for slender beams and it increases up to about 300% for deep beams. Results obtained by higher-order theories are more accurate, the difference from the three-dimensional FEM solution being less than 5% for all the considered values of l/a . The variation of the buckling load

Table 11 Mode II (bending on plane xz) buckling load [MPa], C-shaped cross-section beams

l/a	100	50
FEM 3D	7.4748	29.845
$N = 14$	7.4846, 0.13 ^a	29.887, 0.14
$N = 8$	7.4847, 0.13	29.888, 0.14
$N = 7$	7.4847, 0.13	32.520, 8.96
$N = 6$	7.4847, 0.13	40.347, 35.1
$N = 5$	7.4847, 0.13	45.029, 50.8
$N = 4$	7.4848, 0.13	45.798, 53.4
$N = 3$	7.4850, 0.14	49.622, 66.2
$N = 2$	7.4858, 0.15	49.887, 67.1
TBT	7.4860, 0.15	49.890, 67.1
EBT	7.4881, 0.18	49.980, 67.4

a: Absolute value of the percentage relative error.

versus the half-wave number is shown in Fig. 8 in the case of $l/a = 50$. For $N = 14$, the results match the reference solution, whereas for $N = 6$ the results are inaccurate (this case is not presented for the sake of brevity). Table 11 presents the case of the flexural mode. The buckling load is accurately predicted by classical and low-order theories only in the case of $l/a = 100$. For $l/a = 50$, $N \geq 8$ is required to converge to the reference FEM solution. Classical and low-order theories overestimate the buckling load by about 67%.

6. Conclusions

Several models for the buckling analysis of thin-walled beam structures have been derived via a unified formulation. Via this approach, higher-order theories that account for shear deformations, in- and out-of-plane warping can be formulated straightforwardly. Classical models, such as Euler-Bernoulli's and Timoshenko's, are obtained as particular cases. A closed form, Navier-type solution has been used. Slender and deep beams with several cross-sections (box, C- and I-shaped) have been investigated. Three-dimensional FEM solutions obtained via the commercial code Ansys have been considered as reference solutions. Classical models are accurate only in the case of flexural buckling modes of slender beams. Coupled bending-torsion modes are more difficult to be described accurately and higher approximation order than for the flexural modes are required. It has been shown that the proposed formulation allows obtaining results as accurate as desired through an appropriate choice of the approximation order tackling the complexity due to increasing the expansion order over the beam cross-section.

Acknowledgements

The present work has been supported by the Fonds National de la Recherche Luxembourg via the CORE project C09/MS/05 FUNCTIONALLY.

References

- Basaglia, C., Camotim, D. and Silvestre, N. (2009), "GBT-based local, distortional and global buckling analysis of thin-walled steel frames", *Thin-Wall. Struct.*, **47**(11), 1246-1264.
- Beale, R. G., Godley, M. H. R. and Enjily, V. (2001), "A theoretical and experimental investigation into cold-formed channel sections in bending with the unstiffened flanges in compression", *Comput. Struct.*, **79**(26-28), 2403-2411.
- Bleich, F. (1952), *Buckling Strength of Metal Structures*. McGraw-Hill, New York, USA.
- Camotim, D., Basaglia, C. and Silvestre, N. (2010), "GBT buckling analysis of thin-walled steel frames: A state-of-the-art report", *Thin-Wall. Struct.*, **48**(10-11), 726-743.
- Carrera, E. (2003), "Theories and finite elements for multilayered plates and shells: A unified compact formulation with numerical assessment and benchmarking", *Arch. Comput. Method. E.*, **100**(3), 215-296.
- Carrera, E. and Brischetto, S. (2008a), "Analysis of thickness locking in classical, refined and mixed multilayered plate theories", *Compos. Struct.*, **82**(4), 549-562.
- Carrera, E. and Brischetto, S. (2008b), "Analysis of thickness locking in classical, refined and mixed theories for layered shells", *Compos. Struct.*, **85**(1), 83-90.
- Carrera, E. and Giunta, G. (2009a), "Hierarchical evaluation of failure parameters in composite plates", *AIAA J.*, **47**(3), 692-702.
- Carrera, E. and Giunta, G. (2009b), "Exact, hierarchical solutions for localised loadings in isotropic, laminated and sandwich shells", *J. Press. Vess-T. ASME*, **131**(4), 041202.
- Carrera, E. and Giunta, G. (2010), "Refined beam theories based on a unified formulation", *Int. J. Appl. Mech.*, **2**(1), 117-143.
- Carrera, E. and Giunta, G., Nali, P., and Petrolo, M. (2010), "Refined beam elements with arbitrary cross-section geometries", *Comput. Struct.*, **88**(5-6), 283-293.
- Chen, W.F. and Santathadaporn, S. (1968), *Recent Developments in the Study of Column Behaviour under Biaxial Loading*, Technical Report 331.1, Fritz Engineering Laboratory, Pennsylvania, USA.
- Cowper, G.R. (1966), "The shear co-efficient in timoshenko beam theory", *J. Appl. Mech.*, **330** (10), 335-340.
- Dinis, P.B., Camotim, D. and Silvestre, N. (2006) "GBT formulation to analyse the buckling behaviour of thin-walled members with arbitrarily 'branched' open cross-sections", *Thin-Wall. Struct.*, **44**(1), 20-38.
- Giunta, G., Biscani, F. Carrera, E. and Belouettar, S. (2011) "Analysis of thin-walled beams via a one-dimensional unified formulation", *Int. J. Appl. Mech.*, **3**(3), 407-434.
- Gonçalves, R., Dinis, P.B. and Camotim, D. (2009), "GBT formulation to analyse the first-order and buckling behaviour of thin-walled members with arbitrary cross-sections", *Thin-Wall. Struct.*, **47**(5), 583-600.
- Goodier, J.N. (1942), "Flexural-torsional buckling of bars of open section under bending, eccentric thrust or torsional loads", Cornell University Engineering Experimental Station Bulletin, **28**.
- Kapania, R.K. and Raciti, S. (1989a), "Recent advances in analysis of laminated beams and plates, part I: Shear effects and buckling", *AIAA J.*, **27**(7), 923-934.
- Kapania, R.K. and Raciti, S. (1989b), "Recent advances in analysis of laminated beams and plates, part II: Vibrations and wave propagation", *AIAA J.*, **27**(7), 935-946.
- Kirchhoff, G. (1850), "Über das gleichgewicht und die bewegung einer elastischen sceleibe", *Journal für die reine und angewandte Mathematik*, **50**, 51-88.
- Love, A.E.H. (1888), "The small free vibrations and deformation of a thin elastic shell", *Philos. T. R. Soc. A.*, **179**, 491-546.
- Mohri, F., Azrar, L. and Potier-Ferry, M. (2001), Flexural-torsional post-buckling analysis of thin-walled elements with open sections, *Thin-Wall. Struct.*, **39**(11), 907-938.
- Murty, A.V.K. (1970), "Analysis of short beams", *AIAA J.*, **8**, 2098-2100.

- Nishino, F., Kasemset, C. and Lee, L. (1977) "Variational formulation of stability problems for thin-walled members", *Ingenieur-Archiv*, **43**(1), 58-68.
- Paczos, P. and Wasilewicz, P. (2009), "Experimental investigations of buckling of lipped, cold-formed thin-walled beams with i-section", *Thin-Wall. Struct.*, **47**(11), 1354-1362.
- Put, B. M., Pi, Y. L. and Tahair, N. S. (1999), "Lateral buckling tests on cold-formed channel beams", *J. Struct. Eng.*, **125**(5), 532-539.
- Reddy, J.N. (2004), *Mechanics of Laminated Composite Plates and Shells Theory and Analysis*. CRC Press, Boca Raton, Florida, USA.
- Sauchá, J. and Rados, J. (2001), "A critical review of Vlasov's general theory of stability on in-plane bending of thin-walled elastic beams", *Meccanica*, **36**(2), 177-190.
- Schardt, R. (1983), *The generalized beam theory, chapter Instability and plastic collapse of steel structures* (Proceedings of the M.R. Horne conference, University of Manchester), Granada Publishing, London, UK.
- Schardt, R. (1989), *Verallgemeinerte Technische Biegetheorie*, Springer, Berlin, Germany.
- Schardt, R. (1994), "Generalised beam theory - An adequate method for coupled stability problems", *Thin-Wall. Struct.*, **19**(2-4) 161-180.
- Timoshenko, S.P. (1945) "Theory of bending, torsion and buckling of thin-walled members of open cross section", *J. Franklin I.*, **239**(3), 201-219.
- Timoshenko, S.P. and Goodier, J.N. (1970), *Theory of Elasticity*, McGraw-Hill, New York, USA.
- Trahair, N.S. (1993), *Flexural-Torsional Buckling of Structures*, Chapman and Hall, London, UK.
- Vlasov, V.Z. (1959), *Thin-Walled Elastic Beams*, Fizmatgiz, Moscow, Russia.
- Wagner, H. (1929), *Verdrehung und Knickung von offenen Profilen*, The 25th Anniversary of the Technische Hochschule, Danzig.
- Wagner, H. (1936), "Torsion and buckling of open sections", Technical Memorandum No. 807, U.S.A., National Advisory Committee for Aeronautics.
- Zhang, L. and Tong, G. (2004), "Flexural-torsional buckling of thin-walled beam members based on shell buckling theory", *Thin-Wall. Struct.*, **42**(12), 1665-1687.
- Zhang, L. and Tong, G. (2008), "Elastic flexural-torsional buckling of thin-walled cantilevers", *Thin-Wall. Struct.*, **46**(1), 27-37.